

2D Materials



PAPER

Stabilizing the heavily-doped and metallic phase of MoS₂ monolayers with surface functionalization

RECEIVED

14 June 2021

REVISED

30 November 2021

ACCEPTED FOR PUBLICATION

2 December 2021

PUBLISHED

xx xx xxxxx

Hanyu Zhang¹, Tamara D Koledin¹, Xiang Wang^{2,3}, Ji Hao¹, Sanjini U Nanayakkara¹ ,
Nuwan H Attanayake¹ , Zhaodong Li¹, Michael V Mirkin² and Elisa M Miller^{1,*}

¹ Materials, Chemistry, and Computational Science Directorate, National Renewable Energy Laboratory, Golden 80401, CO, United States of America

² Department of Chemistry, Queens College-CUNY, Flushing, NY 11367, United States of America

³ Chemistry Program, Graduate Center of CUNY, New York, NY 10016, United States of America

* Author to whom any correspondence should be addressed.

E-mail: elisa.miller@nrel.gov

Keywords: MoS₂ monolayers, n-doping, phase conversion, diazonium functionalization, air-stable

Supplementary material for this article is available [online](#)

Abstract

Monolayer molybdenum disulfide (MoS₂) is one of the most studied two-dimensional (2D) transition metal dichalcogenides that is being investigated for various optoelectronic properties, such as catalysis, sensors, photovoltaics, and batteries. One such property that makes this material attractive is the ease in which 2D MoS₂ can be converted between the semiconducting (2H) and metallic/semi-metallic (1T/1T') phases or be heavily n-type doped 2H phase with ion intercalation, strain, or excess negative charge. Using *n*-butyl lithium (BuLi) immersion treatments, we achieve 2H MoS₂ monolayers that are heavily n-type doped with shorter immersion times (10–120 mins) or conversion to the 1T/1T' phase with longer immersion times (6–24 h); however, these doped/converted monolayers are not stable and promptly revert back to the initial 2H phase upon exposure to air. To overcome this issue and maintain the modification of the monolayer MoS₂ upon air exposure, we use BuLi treatments plus surface functionalization p-(CH₃CH₂)₂NPh-MoS₂ (Et₂N-MoS₂)—to maintain heavily n-type doped 2H phase or the 1T/1T' phase, which is preserved for over two weeks when on indium tin oxide or sapphire substrates. We also determine that the low sheet resistance and metallic-like properties correlate with the BuLi immersion times. These modified MoS₂ materials are characterized with confocal Raman/photoluminescence, absorption, x-ray photoelectron spectroscopy as well as scanning Kelvin probe microscopy, scanning electrochemical microscopy, and four-point probe sheet resistance measurements to quantify the differences in the monolayer optoelectronic properties. We will demonstrate chemical methodologies to control the modified monolayer MoS₂ that likely extend to other 2D transition metal dichalcogenides, which will greatly expand the uses for these nanomaterials.

1. Introduction

Molybdenum disulfide (MoS₂) monolayers are a promising material for various applications, such as catalysis, quantum computing, gas sensors, batteries, and biosensors due to the tunable electronic structure, low toxicity, flexibility, and low cost [1–7]. MoS₂ is one of the most studied transition metal dichalcogenides, where the layered materials are held together via van der Waals forces and have optoelectronic properties that are determined by the layer numbers

[8]. It has been shown that MoS₂ monolayers are three atoms thick and have a direct band gap in its thermodynamically stable, semiconducting phase (2H or also referred to as 1H for the monolayer) [9].

To make the most of MoS₂ monolayers, it is essential that the optoelectronic properties are readily controlled and manipulated for any application. As-grown monolayer MoS₂ by chemical vapor deposition (CVD) without intentional doping is typically an n-type semiconducting material; however, this can be tuned by changing growth conditions and growing on

different substrates [10–14]. One such desired property is phase engineering MoS₂ monolayers between its 2H phase and the unstable metallic/semi-metallic (1T/1T') phase using excess negative charge, strain, and defects [5, 15–21]. The 1T MoS₂ monolayer is metallic with an octahedral geometry, whereas the 1T' phase has a small bandgap (theoretically predicted to be 10 s to 100 s meV, depending on the level of theory) [22–24] and a distorted octahedral geometry but still exhibits metallic-like properties [20, 25, 26]. Monolayers of 1T/1T' MoS₂ can be useful because of the low sheet resistance for energy storage as well as an active basal plane for catalysis [5, 27]. Based on previous studies, the 1T phase is not stable and readily relaxes to the 1T' phase; therefore, all the metallic-like MoS₂ monolayers will be referred to as 1T' [22]. In addition to these extremes, MoS₂ can also exist in the 2H phase but be heavily n-type doped, where the Fermi level lies near/at the conduction band minimum and the bandgap is reduced [28–32].

Monolayers can be beneficial over nanosheets (many layers thick) because they are essentially all surface, thinner, and can be grown in large areas. However, there are limited studies explicitly demonstrating good stability of n-type doped 2H phase or 1T' phase MoS₂ monolayers in air [33, 34]. A 2021 report highlighted electron doping MoS₂ monolayers using KOH/benzo-18-crown-6 to stabilize the doped MoS₂ for over one month in air [34]. On the contrary, it has been well documented that MoS₂ nanosheets can be (partially) converted to the 1T' phase and survive for a limited time in air [35–37]. To extend the shelf life and use of these 1T' MoS₂ nanosheets, one strategy is to functionalize the metallic MoS₂ with surface groups to 'lock-in' the metallic properties [38]. In cases where uniform, monolayer coverage with a large lateral area is required or beneficial [31, 39], one must be able to confidently control and manipulate the optoelectronic properties of monolayers—similar to the nanosheets. However, monolayers are more sensitive to their surroundings than nanosheets [25]. Therefore, the focus of this study is to experimentally demonstrate the use of chemical functionalization to control and stabilize the 1T' phase or heavily n-type doped 2H phase of MoS₂ monolayers.

Here, we manipulate MoS₂ monolayers from 2H to heavily n-type doped 2H to 1T' using *n*-butyl lithium (BuLi) immersion treatments, where BuLi has been used to phase convert MoS₂ monolayers previously and is based on bulk MoS₂ exfoliation [38, 40, 41]. A shorter BuLi immersion time (10–120 mins) heavily n-type dopes MoS₂ while a longer BuLi immersion time (>2 h) converts the MoS₂ from 2H to 1T' phase when the monolayers are supported on indium tin oxide (ITO) or sapphire substrates. We show with various spectroscopic, microscopic, and electronic transport techniques that the heavily n-type doped 2H/1T' phase is not stable

in air and reverts back to the initial 2H phase before the appropriate measurements can be performed. To stabilize the n-type doped 2H and 1T' phase, we functionalize the surface using a diazonium salt to form (CH₃CH₂)₂NPh-MoS₂ (Et₂N-MoS₂). Our various characterization techniques confirm that the heavily n-type doped 2H and 1T' phase is maintained in air and that the degree of sheet resistance can be tuned by the BuLi immersion time. The addition of Et₂N functional groups to MoS₂, allows the heavily n-type doped 2H and 1T' phase of MoS₂ monolayers to be used in air, which could be more readily incorporated into various nanodevices.

2. Materials and methods

2.1. Single crystal monolayer growth

Si with 300 nm thermal oxide layer (University Wafers) was cut and annealed in a 550 °C oven for 10 min. The substrate was spin-coated with 300 μl of precursor—made up of supernatant saturated MoO₃ (Sigma Aldrich, 99.97% purity, powder) and 0.02 M NaOH solution (Fisher Scientific, ≥97.0% purity pellets) with ultrapure water (18.2 MΩ)—at 1600 rpm for 50 s. Single crystal monolayer MoS₂ was grown via CVD in a three-chamber furnace under atmospheric pressure (625 Torr) with a 50 sccm argon gas flow. The method is modified from a previous report [42]. The furnace temperatures were 530 °C, 800 °C, and 800 °C for zone 1, 2, and 3, respectively, with a ramp-up rate at 35 °C min⁻¹. The precursor loaded silicon substrate was placed in the end of the third zone. Solid sulfur precursor pellets were placed upstream in an alumina boat, and the closed system was purged with argon three times. The sulfur was heated to 180 °C for 8 min with heat tape when zone 3 of the furnace reached 700 °C. The furnace and heat tape were turned off, and the sample was left to cool with argon flow until the furnace temperature was 150 °C. This process resulted in single crystal, isolated triangles of MoS₂ monolayers with sizes up to 30 μms. The single-crystal monolayer MoS₂ samples were characterized by photoluminescence (PL) spectroscopy, x-ray photoelectron spectroscopy (XPS), scanning Kelvin probe microscopy (SKPM) and scanning electrochemical microscopy (SECM).

2.2. Transfer of single crystal monolayer MoS₂ to substrates

A polystyrene solution (PS, average molecular weight ~192 000, Sigma-Aldrich) was spin-coated on the MoS₂ grown Si sample at 3000 rpm for 60 s. The PS coated sample was put in a 150 °C oven for 5 min, and then the edges were scratched with a razor blade. The PS/MoS₂ sample on Si/SiO₂ was slowly immersed in 80 °C 2 M NaOH solution until the PS/MoS₂ film fully peeled off from the Si/SiO₂. The floating film was then fished out with a glass slide, and transferred into ultrapure water, and lastly extracted with the new

substrate, i.e. ITO. The sample was soaked in toluene for 20 min, rinsed with ultrapure water, and annealed in an N₂ environment for 30 min at 200 °C.

2.3. Continuous-film monolayer growth

Continuous monolayer MoS₂ was adapted from a previous report [43]. The large-area MoS₂ was grown in a 1 Torr CVD environment with an argon flow of 80 sccm and argon with 4% O₂ at 6 sccm. A precursor, 2 mg MoO₃, was placed in zone 2 of the furnace. Approximately 2 g of sulfur was placed prior to zone 1. A <0001> sapphire wafer (University Wafer) was used and bath-sonicated in acetone, isopropanol, and ultrapure water for 10 min each before being placed at the end of zone 3. The closed system was purged with argon three times and the furnace was heated to 530 °C, 930 °C, and 930 °C for zone 1, 2 and 3, respectively. The temperatures were maintained for 35 min before turning off the furnace. The system was left to cool with argon flow until the furnace reached 150 °C. The continuous monolayer MoS₂ samples on as-grown on sapphire were used for UV-Vis absorption and four-point probe measurements.

2.4. Doping/converting 2H MoS₂ and surface-functionalization

The 2H MoS₂ monolayers were immersed into fresh 2.5 M BuLi (Sigma Aldrich) for various times in a N₂ glovebox. To achieve repeatable results, the BuLi had to be fresh without any visible precipitates. BuLi solution residue can be removed by hexane (Sigma Aldrich). To add functional groups to the MoS₂, the BuLi treated monolayers were immediately put into 10 mg ml⁻¹ 4-p-diazo-N,N-diethylaniline fluoroborate (MP Biomedicals) aqueous solution for 30 min. The functionalized monolayer samples were immersed into 50 ml isopropyl alcohol (J T Baker) and rinsed two times with 100 ml ultrapure water sequentially to remove the excess or weakly bound aniline groups. The resulting sample films were then characterized.

2.5. X-ray XPS

Single crystal MoS₂ monolayer films transferred onto ITO were transferred to the XPS setup via an air-free transfer vessel. XPS data were obtained on a Physical Electronics 5600 system using Al K α radiation. The XPS setup was calibrated with Au metal, which was cleaned via Ar-ion sputtering. The raw atomic concentration has a 5% error due to surface inhomogeneities, surface roughness, literature sensitivity values for peak integration, etc. The air-free films were measured under ultra-high vacuum (10⁻⁹ Torr), then the samples were removed from the vacuum and set on the lab bench for 20 mins before being measured again under ultra-high vacuum.

2.6. UV-Vis absorption spectroscopy

The absorption was collected by Cary 5000 series UV/Vis spectrophotometer (Agilent Technologies). The inert environment was achieved by the airtight sample holder with transparent windows. The samples used for these measurements were as-grown continuous MoS₂ monolayers on sapphire.

2.7. Confocal Raman spectroscopy and PL

Raman and PL spectroscopy was performed on a Renishaw inVia (Gloucestershire, UK) by using a 532 nm laser and 100 \times magnification or 50 \times long working distance objective lenses. The scattering light from the sample was directed by a grating with 1800 lines mm⁻¹ for Raman or 600 lines mm⁻¹ for PL prior to the CCD detector. The Raman/PL mapping is achieved by a motorized stage with 0.3 μ m step size. The typical exposure time is 2 s with five accumulations to reduce the instrumental noise. The samples used here were single crystal MoS₂ monolayer films transferred onto ITO. For the air-free measurements, we used an airtight sample holder with transparent windows.

2.8. SKPM

SKPM measurements were performed in air using single pass mode on a Park atomic force microscopy (AFM) equipped with an XE-70 controller and an external lock-in amplifier (SR830, Stanford Research Systems). Measurements were made with an electrical AC bias applied on the tip, using lock-in detection and feedback at 18 kHz for the surface potential signal. Conductive Pt/Ir-coated AFM cantilevers (Multi-75EG, Budget Sensors) were used for SKPM imaging. Topography was measured at the first resonance frequency (\sim 70 kHz) and potential was collected with a 1.00 V AC bias at 18 kHz, well-separated from the topography frequency.

2.9. SECM

SECM experiments were carried out using the home-built setup as described previously [44], including the three-electrode setup with a 0.25 mm diameter Ag wire coated with AgCl serving as a reference electrode, a 1 mm Pt wire counter electrode, and an unbiased substrate. Pt nanoelectrodes with the tip radius, $a \approx$ 120 nm (calculated from the diffusion-limited current of 1 mM ferrocenemethanol), were fabricated by pulling and heat sealing 25 μ m diameter Pt wires into borosilicate glass capillaries under vacuum with a P-2000 laser pipet puller. The fabricated nanoelectrodes were polished on a 50 nm alumina pad (Precision Surfaces International) under video microscopic control. Appropriate protection was used to avoid electrostatic damage to the nanotips.

The tip was brought within about 30 μ m vertical distance from the substrate using a manual micromanipulator and an optical microscope. Then,

the tip was moved toward the substrate using the z piezo stage over $\sim 25 \mu\text{m}$ distance with a relatively high approach velocity (e.g. $0.5 \mu\text{m s}^{-1}$). An approach curve was obtained with a slower velocity (e.g. 40 nm s^{-1}). All experiments were carried out at room temperature inside a Faraday cage.

Feedback mode of the SECM operation was used to image the monolayers. In feedback mode, the SECM probe was brought within a short distance from the MoS_2 monolayer immobilized on a flat, conductive ITO surface. The electrolyte contained a redox mediator ferrocenemethanol (Fc), and the tip potential (E_T) was such that the mediator oxidation occurred at a rate governed by diffusion. With the separation distance between the tip and substrate (d) sufficiently small (i.e. comparable to a), the oxidized form of the mediator (Fc^+) produced at the tip surface was reduced at the substrate, and the tip current increased with decreasing d (positive feedback; the tip current near the surface was higher than its value in the bulk solution; $i_T > i_{T,\infty}$). If the regeneration rate of the mediator at the substrate was slow, i_T decreased with decreasing d because of the hindered diffusion of Fc (negative feedback; $i_T < i_{T,\infty}$). An image was obtained by scanning the tip laterally (in the x - y plane) over the sample surface.

2.10. Four-point probe measurements

The typical four-point probe measurement was performed by using Signatone four-point resistivity measurement system with a custom-developed LabVIEW program. All measurements were conducted inside the N_2 -filled glovebox in the dark. For each sample on the sapphire substrate, current vs. voltage curves of at least five different positions were measured and recorded.

3. Results and discussion

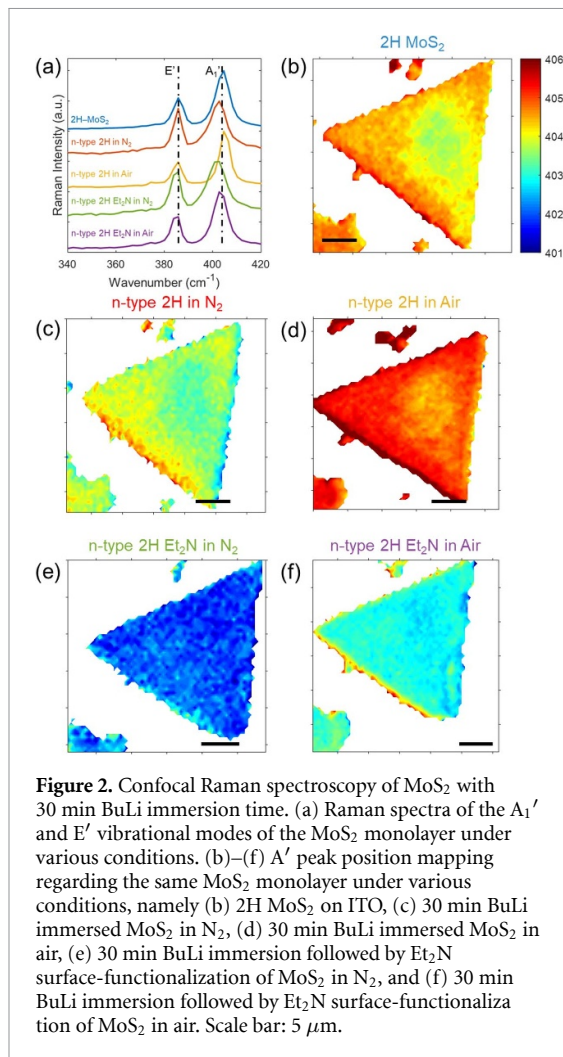
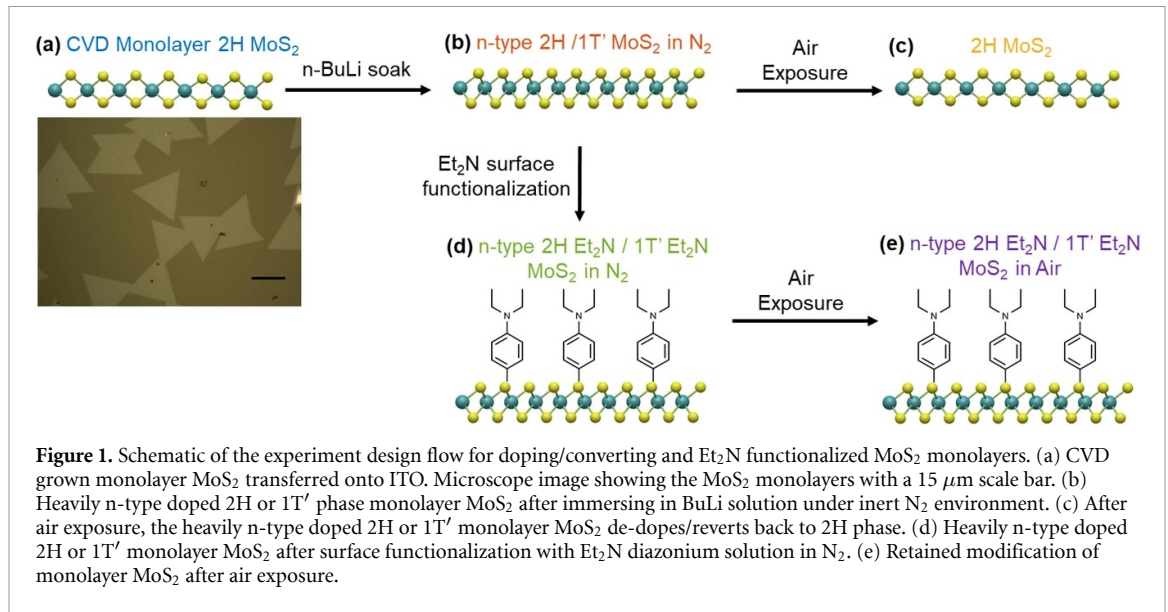
In order to stabilize the heavily n-type doped 2H and 1T' phase of MoS_2 monolayers in air, we develop a modified protocol based on a previous report with BuLi treatments and surface functionalization (figure 1) [38]. For these studies, we use CVD grown monolayers of 2H MoS_2 (figure 1(a)), which can be transferred from the growth substrate Si/SiO_x onto other substrates if needed for characterization; the monolayer growth and transfer are detailed in the section 2. The transferred MoS_2 monolayers onto ITO or the continuous film MoS_2 monolayers on sapphire maintain the thermodynamically stable 2H phase until we intentionally alter it with BuLi immersion treatments. As shown in the schematic in figure 1, we start with 2H MoS_2 (figure 1(a)) and immerse the monolayer film in BuLi in a N_2 glovebox to convert the MoS_2 from 2H to heavily n-type doped 2H or 1T' phase (figure 1(b)). Once the monolayer is exposed to air, the MoS_2 de-dopes/converts back to the initial 2H (figure 1(c)). To stabilize the

heavily n-type doped 2H or 1T' phase, we add Et_2N functional groups to the monolayer in the glovebox (figure 1(d)), which stabilizes the materials for at least two weeks in air (figure 1(e)). The doping/phase of the MoS_2 monolayers is measured using UV-Vis absorption spectroscopy, confocal PL spectroscopy, and XPS (figure 4) as well as Raman spectroscopy (figures 2 and 7). We confirm the materials are monolayer by the splitting of the A_1' and E' Raman features (figure 2(a)), the strong PL (figure 3(b)), and AFM measurements (figure 5). Note that our CVD growth does not produce exclusively MoS_2 monolayers; therefore, the UV-Vis absorption, XPS, and four-point probe measurements may have some signal from multilayer growth that is within our measurement detection area.

3.1. 30 min BuLi immersion time

Raman spectroscopy is a valuable tool for evaluating MoS_2 layer thickness, phase, and doping. For these studies, we use confocal Raman microscopy with one-micron spatial resolution to characterize the MoS_2 monolayers following various treatments. Monolayer MoS_2 has the point group D_{3h} [45]. Therefore, A_1' and E' are used to identify the out-of-plane and in-plane stretching modes, respectively, instead of A_{1g} and E_{2g} that are used for multilayers. Our transferred 2H MoS_2 has a $\sim 18.6 \text{ cm}^{-1}$ A_1'/E' splitting, which is in agreement with a monolayer (figure 2(a)) [46]. Once the monolayer is treated with BuLi for 30 mins, we measure the Raman spectrum in a N_2 environment to determine if the monolayer has been electron doped or phase converted. The A_1' peak red shifts by $\sim 1.7 \text{ cm}^{-1}$, while the E' peak position is constant, which has been recently shown to be attributed to n-type doping of MoS_2 monolayers [33]. Furthermore, we do not observe the typical J peaks associated with the 1T/1T' phase of MoS_2 (extended spectra shown in figure S1 available online at stacks.iop.org/2DM/00/00000/mmedia) [47, 48]. The A_1' red shift and lack of J peaks is a result of softened out-of-plane vibrations through weakening S-Mo bonds due to electron density occupying the antibonding states in the conduction band, yet not enough electron transfer for phase conversion to 1T/1T' with a 30 min BuLi immersion treatment [29, 49]. Note, we will expand upon this n-type doped 2H/1T' phase differentiation more in the next section.

To closely evaluate how the 30 min BuLi immersion and functionalization affects the MoS_2 monolayer, we use Raman mapping of the same MoS_2 triangle following each treatment. For the 2H MoS_2 sample, the A_1' peak position has a small ($\sim 1 \text{ cm}^{-1}$) variation around 404 cm^{-1} across the entire monolayer, which provides us with a baseline (figure 2(b)). Following a 30 min BuLi immersion time, the A_1' mapping (figure 2(c)) reveals that the peak is evenly red-shifted ($\sim 403 \text{ cm}^{-1}$) and that n-type doping is throughout the monolayer. The E' peak position is



unaffected by the BuLi treatment and results in an A₁'/E' splitting of ~17.1 cm⁻¹ (figure 2(a)). Once the MoS₂ monolayer is exposed to air, the A₁' peak blue shifts to ~405 cm⁻¹ (figure 2(d)), which is slightly

higher (~0.5 cm⁻¹) than the initial 2H MoS₂ and is probably due to the de-doped monolayer becoming slightly oxidized (see XPS results below). Likely, this de-doping is an electron-withdrawing process via an oxidizing agent in air (i.e. O₂ or H₂O molecules) [50]. Therefore, when considering MoS₂ monolayers, the fact that we cannot even perform the measurements before the sample reverts to the initial 2H MoS₂ is noteworthy and would be challenging to use if heavily n-type doped 2H MoS₂ monolayers are needed in an air-exposed application.

In our previous MoS₂ nanosheets study, we were able to elongate the shelf-life of the 1T/1T' MoS₂ nanosheets with surface functionalization [38]. Therefore, taking notes from this previous study, we use surface functionalization to extend the lifetime of the modified MoS₂ monolayers in air. Specifically, we use the BuLi treated monolayers in a glove box and immerse the film into 4-p-diazo-N,N-diethylaniline fluoroborate aqueous solution. This results in bound p-(CH₃CH₂)₂NPh functional groups to the n-type doped 2H MoS₂ monolayer, where the n-type 2H Et₂N-MoS₂ samples are kept under a N₂ environment for the Raman measurements. The A₁' peak red shifts by ~2.7 cm⁻¹ and the E' slightly red shifts by ~0.8 cm⁻¹ (figure 2(e)). Therefore, the ~16.9 cm⁻¹ A₁'/E' splitting along with the greater red shift of A₁' leads us to conclude that Et₂N functionalized MoS₂ in air is also heavily n-type doped and that the surface functionalization results in an overall ~1 cm⁻¹ red shift. Once the monolayer is exposed to air, the mapping data reveals the n-type 2H Et₂N-MoS₂ in air is homogeneously n-type doped throughout the monolayer (figure 2(f)), with only a small blue shift of A₁' compared to the sample in N₂. The Raman spectroscopy allows us to determine the 30 min BuLi immersion time results in heavily n-type doping of the MoS₂ monolayers that is

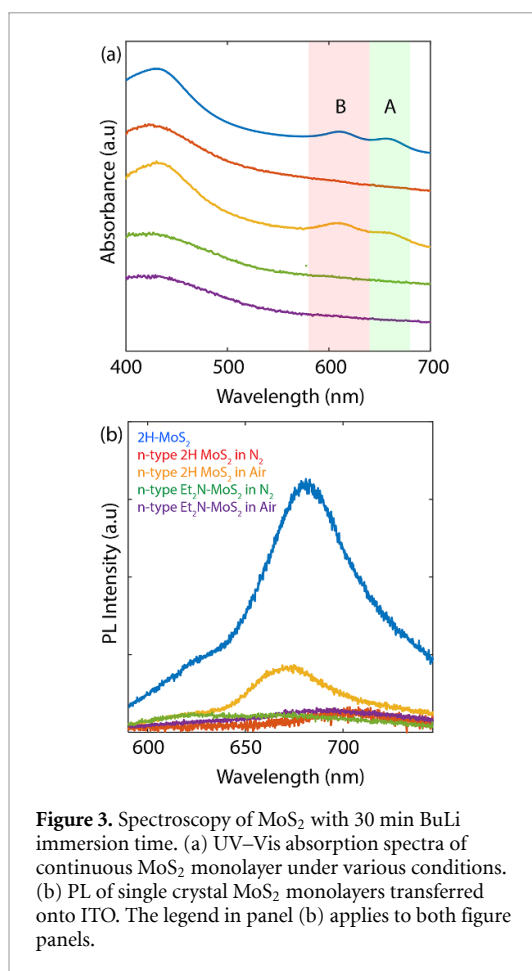


Figure 3. Spectroscopy of MoS₂ with 30 min BuLi immersion time. (a) UV-Vis absorption spectra of continuous MoS₂ monolayer under various conditions. (b) PL of single crystal MoS₂ monolayers transferred onto ITO. The legend in panel (b) applies to both figure panels.

stabilized in air when functionalized with Et₂N. Other characterization techniques are used to measure the 30 min BuLi treated MoS₂ monolayers.

The monolayer A and B exciton features are well-known indicators for the direct bandgap, semiconducting 2H phase of MoS₂, which reflects the spin-orbit splitting of the valence band maximum at the K point in the Brillouin zone. In figure 3(a), the absorption spectrum of continuous MoS₂ (2H-MoS₂) monolayer shows clear A and B exciton transitions at ~610 and ~660 nm, which matches the previous reports for monolayer MoS₂ [51]. After immersing the monolayers in BuLi for 30 min (figure 3(a)), both the A and B exciton features disappear as long as the treated monolayers remain in an inert environment. The loss of the exciton features is expected due to electron transfer from the strong reducing agent (BuLi) to MoS₂ [52–54]. The n-type doped 2H MoS₂ monolayer sample is unstable when exposed to ambient air. The A and B excitons start to grow in as the MoS₂ de-dopes back to the initial doping level during the UV-Vis absorption measurement when performed under ambient conditions (figure 3(a)). These absorption measurements take ~10 min, which is enough time to restore the A and B exciton features back to the intensity of the initial 2H phase of MoS₂.

Upon surface functionalization and air exposure, the A and B excitons of MoS₂ are still suppressed (figure 3(a)), which indicates the surface functionalization maintains the n-type doping. The A and B exciton features remain relatively suppressed for several weeks as the A and B excitons slowly grow in under ambient conditions (figure S2). Our results demonstrate that the surface functionalization provides a unique way to maintain the heavily n-type doping of MoS₂ monolayers for at least two weeks and likely longer, which will be a focus of future studies.

To further confirm the stabilization of the n-type doped 2H phase of MoS₂ monolayers, we use confocal PL, where we measure the PL from one monolayer triangle (figure 3(b)). The initial 2H MoS₂ (transferred onto ITO) demonstrates the highest PL intensity at ~680 nm and corresponds to emission from the A exciton [34]. The A exciton emission is quenched when the monolayers are treated with BuLi for 30 mins, which is similar to previous n-type doping experiments [34, 55]. However, the PL grows in when the n-type doped 2H phase MoS₂ monolayers are exposed to air. The PL is blue-shifted by 5 nm (~675 nm) and is likely due to a slightly oxidized surface (see XPS results). By adding Et₂N functional groups to the BuLi treated monolayers, the PL remains minimized in N₂ and ambient air conditions (figure 3(b)). These results strongly agree with the Raman and UV-Vis absorption data and demonstrate the stability of n-type doped 2H phase MoS₂ monolayers in air when adding the Et₂N functional groups.

Similar conclusions can also be drawn from the XPS results. We measure two samples one where the transferred MoS₂ monolayers are treated with BuLi for 30 mins and one where the monolayers are treated with BuLi for 30 mins followed by aqueous 4-p-diazo-N,N-diethylaniline fluoroborate in a glovebox. These samples are subsequently transferred air-free to the XPS setup and measured with XPS (figures 4(b) and (d)). Once XPS measurements on the air-free samples are complete, the same samples are exposed to air for 20 mins on the lab benchtop before re-measuring with XPS (figures 4(c) and (e)). We also have a reference 2H MoS₂ sample for comparison (figure 4(a)). For these measurements, we have a detection area of ~1 mm²; therefore, the XPS data are mostly MoS₂ monolayers but can also contain few layer triangles.

The structural phase and/or doping of MoS₂ can be determined by the Mo⁺⁴ peak positions, where Mo 3d transitions have two peaks due to spin-orbit coupling that are split by 3.13 eV. The XPS data show two distinct Mo⁺⁴ environments for all treated MoS₂ monolayers: an environment consistent with intrinsic 2H (i-2H: 229/232 eV) and a lower binding energy peak, which we attribute to heavy n-type doping (n-2H: 228/231 eV—will be explained in more detail below). By fitting the Mo⁺⁴ peaks, we quantify

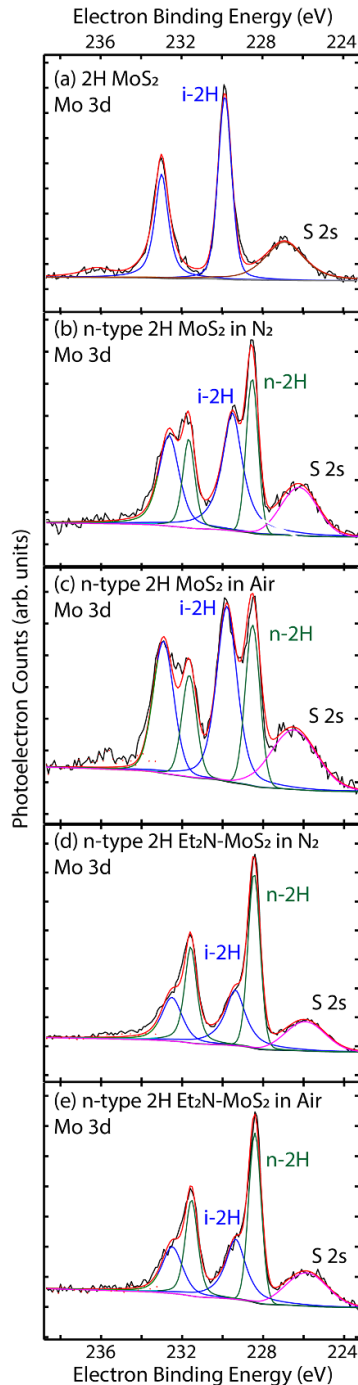


Figure 4. XPS of the Mo 3d region of MoS₂. (a) XPS of untreated 2H MoS₂ is shown for reference. Also, XPS of 30 min BuLi treated MoS₂ in (b) N₂ then (c) exposed to air for 20 min is shown. Similarly, the 30 min BuLi treated plus Et₂N functionalized MoS₂ in (d) N₂ and then (e) exposed to air for 20 min is shown. The lowest energy peak is due to S 2s, which overlaps with the Mo 3d spectra. The Mo 3d spectra is fit to two different types of Mo⁺⁴ environments: i-2H and n-2H.

the amount of n-2H vs i-2H MoS₂ character, where the fits are shown in figure 4. As reference, we only observe the peak of i-2H environment from untreated 2H MoS₂. For the 30 min BuLi treated MoS₂ in N₂, the XPS data yields ~50% n-2H to 50% i-2H MoS₂ character. After exposing the sample to air for 20 mins, our measurements show that the i-2H character increases:

~40% n-type 2H to 60% i-2H MoS₂ character. However, with Et₂N surface functionalization of n-type 2H MoS₂, the XPS Mo 3d spectra are similar between the air-free and air-exposed monolayers, ~65% n-2H to 35% i-2H MoS₂.

Overall, the n-type 2H Et₂N-MoS₂ sample has more n-2H character than the unfunctionalized, 30 min-BuLi treated MoS₂ monolayer (figure 4). The different ratios between the air-free samples emphasize the instability of the unfunctionalized, n-type doped 2H MoS₂ monolayer, where it starts to revert to its initial 2H state during our air-free transfer, which can be a few hours before we perform the XPS measurement. These results agree with the UV-Vis absorption and PL data—emphasizing that the Et₂N surface functionalization stabilizes the n-type doped 2H phase.

If the 30 min BuLi treatment simply n-type doped the MoS₂ monolayers, we would expect the 2H MoS₂ peaks to shift to higher binding energy, which is typical for n-type doping [56, 57]. However, this is not what we measure. What we observe are peak positions that are lower in electron binding energy and similar to 1T/1T' MoS₂ peak positions (228/231 eV) [37, 58]. Therefore, the XPS results suggest that the electron doping collapses the bandgap. According to theoretical reports on degenerately n-type doping 2H MoS₂ monolayers, the bandgap does not collapse but decreases by a few 100 meV [59, 60]. Therefore, a likely explanation is electron doping strains the 2H MoS₂ lattice, which together with electron doping collapses the 2H bandgap and results in the lower electron binding energy XPS features. This conclusion is in alignment with previous MoS₂ studies evaluating the correlation between strain and electron doping [12, 53, 61]. Additional high-resolution microscopy studies (e.g. transmission electron microscopy or scanning tunneling microscopy) are needed to confirm this hypothesis and are beyond the scope of this work.

In addition to Mo 3d spectra, we also acquired S 2p (figure S3(a)) and N 1s spectra (figure S3(b)) of the MoS₂ monolayers. The S 2p has spin-orbit peaks that are separated by 1.18 eV. Like Mo 3d, the S 2p peak positions are dependent on the MoS₂ character, where lower energy transitions (~161.5 eV) have n-2H character and the higher binding energy transitions (~162.5 eV) have i-2H character. As expected, the S 2p peak positions trend similarly to the Mo 3d peak positions. The S 2p spectra show a slight oxidation of the n-type 2H MoS₂ monolayers compared to the n-type 2H Et₂N-MoS₂, resulting in higher binding energy features (~168 eV). For the unfunctionalized n-type doped 2H MoS₂ sample, the increased oxidation and 2H component stress the instability and reactivity of this MoS₂ compared to the functionalized monolayer. We also evaluated the N 1s spectra to confirm the Et₂N functional group. For the n-type 2H Et₂N-MoS₂ monolayer spectrum, we assign the N 1s

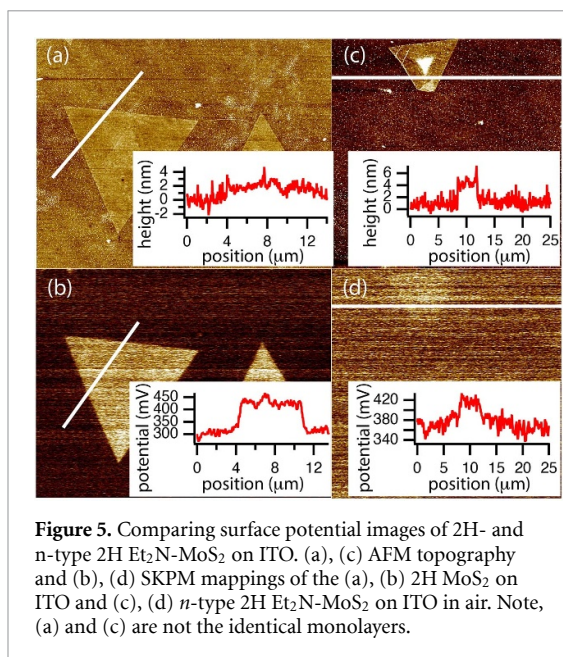


Figure 5. Comparing surface potential images of 2H- and n-type 2H Et₂N-MoS₂ on ITO. (a), (c) AFM topography and (b), (d) SKPM mappings of the (a), (b) 2H MoS₂ on ITO and (c), (d) n-type 2H Et₂N-MoS₂ on ITO in air. Note, (a) and (c) are not the identical monolayers.

peak at ~ 400 eV to the Et₂N functional group based on previous aniline assignments [38, 62].

The Et₂N functionalization stabilizes the change produced by the BuLi, which is similar to what we and others observed with MoS₂ nanosheets, giving a longer ‘shelf life’ [37, 38]. We argue that when the surface group (Et₂N) binds to the surface, it does so by removing negative charge from the monolayers. The combination of the bound functional group and less negative charge on the monolayer ‘locks-in’ the n-type doping or metallic phase and prevents ambient air (H₂O, O₂, CO₂) from interacting with the surface via adsorption/reaction/oxidation. Overall, the functionalization group de-energizes and prevents any rapid oxidation in air.

To further corroborate the uniform doping across the exposed top surface of these layers, we used SKPM, an AFM based technique to map the local surface potential variations and elucidate any changes to the electronic character of the 2H MoS₂ monolayers compared to the n-type 2H Et₂N-MoS₂ monolayers. In addition to acquiring local surface potential information from SKPM, we are also able to measure the apparent height of the measured triangles (figures 5(a) and (c)). The 2H MoS₂ height is ~ 1 nm and strongly suggests a monolayer. Note our AFM measurements are affected by the ITO surface roughness and transfer process. However, our PL/Raman measurements corroborate the existence of monolayer MoS₂ of the transferred samples. As expected, the apparent height of the n-type 2H Et₂N-MoS₂ monolayer is greater due to the BuLi and surface functionalization treatment.

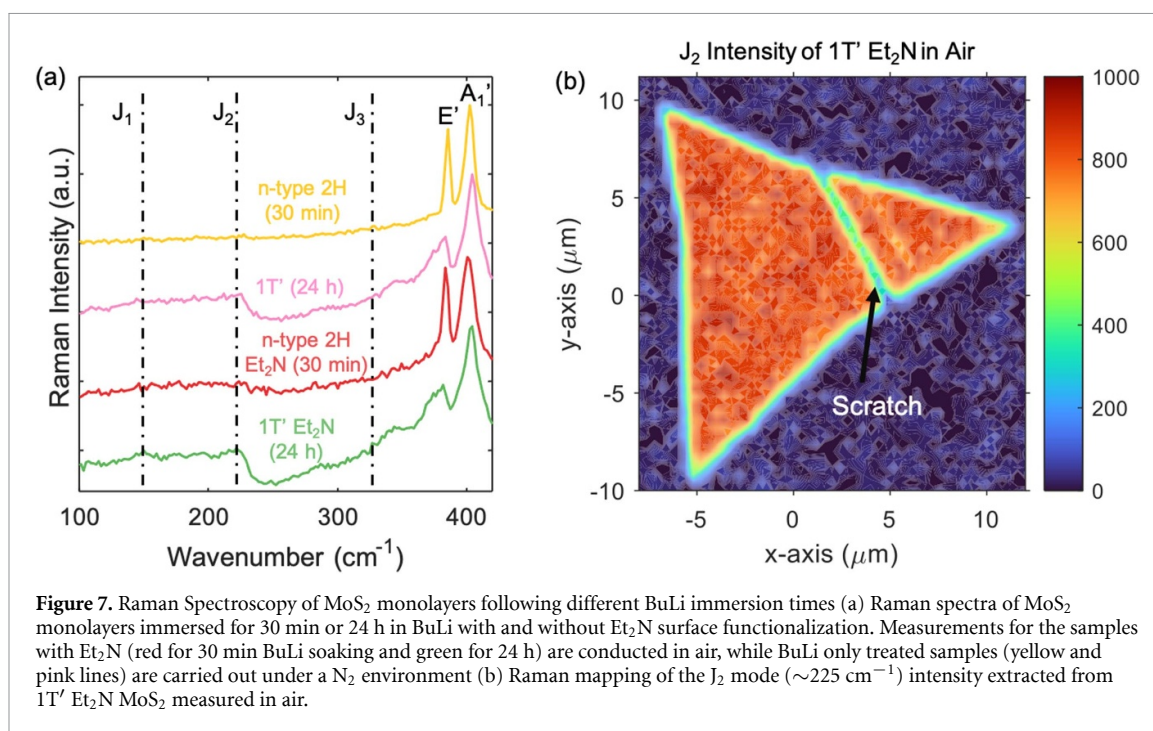
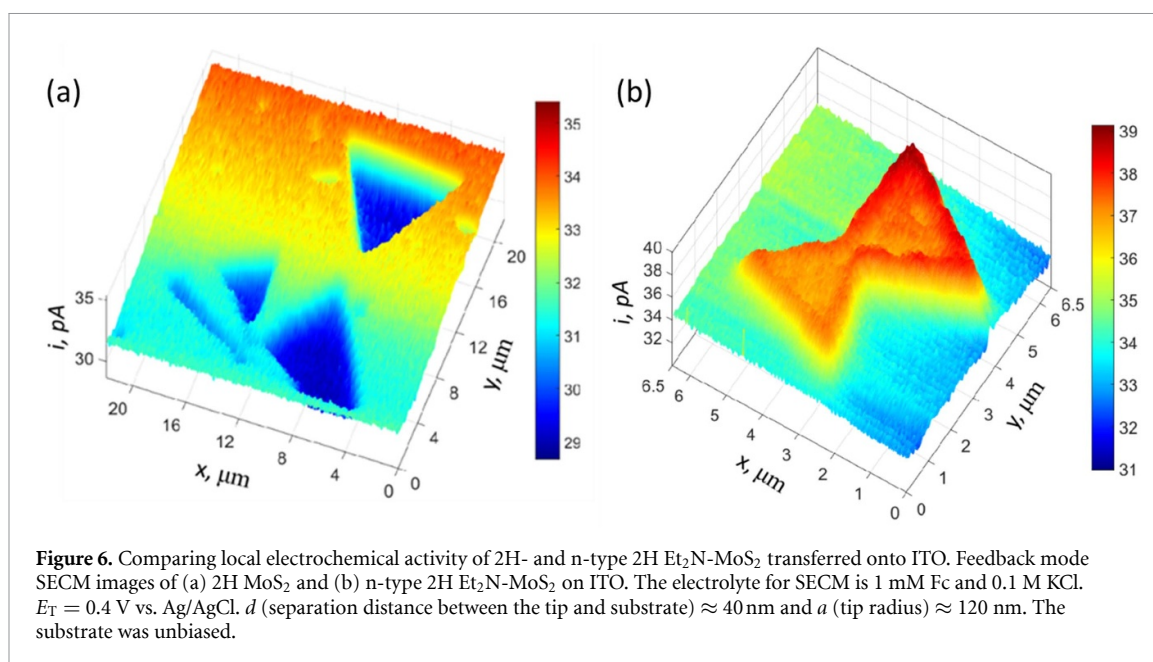
SKPM measures surface potential via detection of electrostatic forces between a conducting probe tip and the surface resulting in images that show the contact potential differences [63]. Thus, this technique

can be used to elucidate qualitative, spatially resolved changes in surface potential resulting from surface functionalization. Furthermore, SKPM has a lateral resolution of ~ 50 nm and thus any variations greater than 50 nm in doping can be resolved. Surface potential images of 2H MoS₂ and n-type 2H Et₂N-MoS₂ are shown in figure 5, where images are not of the same monolayer. The 2H MoS₂ has a surface potential difference from the ITO substrate ($\sim +150$ mV, figure 5(b)). This is different from the n-type 2H Et₂N-MoS₂ monolayer that has close ($\sim +40$ mV) to the same potential as the ITO substrate (figure 5(d)). We use this data to qualitatively conclude that the monolayers have been uniformly modified by Et₂N surface functionalization (additional SKPM data of 2H and n-type 2H Et₂N MoS₂ samples are shown in figure S4). These SKPM results highlight how the 30 min BuLi and Et₂N surface functionalization treatment change the local workfunction uniformly across the monolayers, which could be beneficial for heterostructure energetic alignment in different applications.

To further characterize the flake surface, we use SECM to examine the local chemical reactivity differences. The single crystal 2H-MoS₂ and n-type 2H Et₂N-MoS₂ samples are prepared on ITO at NREL and shipped to CUNY-Queens for SECM measurements under ambient conditions. Figures 6(a) and (b) show the electrochemical activity of 2H-MoS₂ and n-type 2H Et₂N-MoS₂ monolayers, respectively, imaged in the feedback mode. The sample is unbiased, and the tip biased at $E_T = +400$ mV (vs. Ag/AgCl) is positioned over the underlying ITO surface ($d \approx 40$ nm), where the oxidation of Fc is diffusion controlled. The tip current is lower over 2H MoS₂ (29–30 pA) than that over the ITO surface (>31 pA) (figure 6(a)) because the regeneration of the Fc mediator at the insulating 2H MoS₂ is slower than that at the ITO surface. However, the tip current (>36 pA) over the n-type 2H Et₂N-MoS₂ monolayer (figure 6(b)) is higher than that over the ITO background. These measurements inform us that the n-type 2H Et₂N-MoS₂ preserves its high conductivity after the sample is shipped across the country to another lab under ambient conditions (over two weeks from prep to measurement). These results agree with our previous publications showing that n-type 2H Et₂N-MoS₂ is stable under electrochemical conditions and have the potential to be better suited for catalytic reactions [38].

3.2. BuLi immersion time study

As we indicated earlier, the BuLi immersion times impact the degree of doping and phase conversion. In figure 7 and S5, we explore this further with various BuLi immersion times using Raman spectroscopy. The 30 min to 24 h BuLi immersion times are compared with and without Et₂N functionalization (figure 7(a)). For the BuLi only treated MoS₂ monolayers at 30 min and 24 h immersion times, there



is a significant difference between the Raman spectra. The 24 h immersion time yields the characteristic metallic J₁ and J₂ or LA peaks at ~ 150 cm⁻¹ and ~ 225 cm⁻¹, respectively [48, 64, 65]. In general, the 24 h BuLi spectrum is congested and broadened compared to the 30 min immersion time; therefore, the J₃ peak at 320 cm⁻¹ could be present but not large enough to identify. The shoulders at ~ 290 cm⁻¹ and ~ 350 cm⁻¹ are also characteristic of the 1T/1T' phase and have been previously assigned to 1T/1T' MoS₂ phase [48]. In addition, we observe a red shift, decrease in peak intensity, and broadening of the in-plane E' peak (~ 385 cm⁻¹), which has been observed previously for 1T/1T' phases [66, 67]. The significant

and reproducible spectral differences between the 30 min and 24 h BuLi immersion times lead us to conclude that the longer immersion time fully converts the 2H MoS₂ to 1T' phase, whereas the shorter immersion time is an intermediate point that is heavily n-type doped 2H.

To stabilize the 1T' phase conversion from 2H, we add Et₂N surface functional groups. Figure 7(a) compares the 1T' Et₂N-MoS₂ to the unfunctionalized, 1T' MoS₂ at 24 h BuLi immersion times, where the 1T' Et₂N-MoS₂ (24 h) spectrum changes slightly but still has most of the characteristic 1T/1T' features, e.g. J₂ at 225 cm⁻¹, 350 cm⁻¹, and broadened red-shifted E'. Therefore, we conclude that the 1T' Et₂N

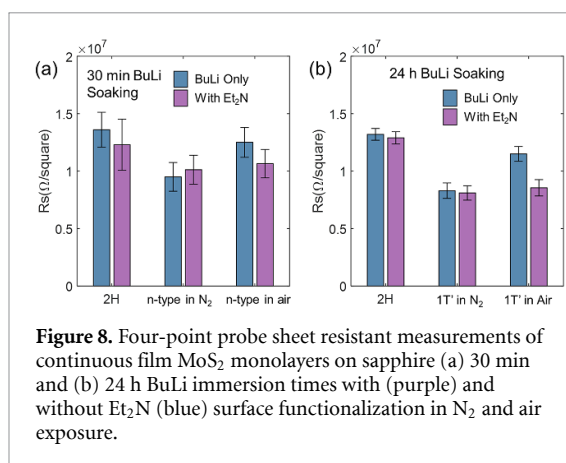


Figure 8. Four-point probe sheet resistant measurements of continuous film MoS₂ monolayers on sapphire (a) 30 min and (b) 24 h BuLi immersion times with (purple) and without Et₂N (blue) surface functionalization in N₂ and air exposure.

functionalized MoS₂ with a 24 h BuLi immersion time remains in the 1T' phase. The J₂ peak intensity is mapped across the 1T' Et₂N-MoS₂ (24 h) monolayer to show that the phase conversion is across the monolayer (figure 7(b), figure S6 for the intensity at 380 cm⁻¹ and 405 cm⁻¹). Additional Raman measurements where the BuLi immersion time is varied, shows that the n-type doping occurs with less than 10 mins BuLi immersion time and the phase conversion happens between 2 h and 6 h immersion times (figure S5). The Raman measurements are critical in differentiating between MoS₂ monolayers being heavily n-type doped or converted to the 1T' phase, whereas UV-Vis absorption, PL, and XPS did not show differences between the BuLi immersion times. Note that when the MoS₂ monolayers are on the Si/SiO_x substrate, the surface protection of 1T' MoS₂ from Et₂N functionalization is not as effective as on ITO or sapphire substrates (figure S7). Understanding this difference in substrate effect will be a focus of upcoming studies, and we speculate it is due to surface adhesion effects.

Finally, the standard four-point probe measurements are performed on the treated MoS₂ monolayers to determine the variation of sheet resistance and stability of these BuLi treated monolayers when exposed to air. Here, we use the continuous growth method for the MoS₂ monolayers on sapphire, and all four-point probe measurements are performed in a N₂ glovebox. For each panel in figure 8, two monolayer samples are used, where the same sample is measured three times: the as grown 2H MoS₂, following treatments(s) in N₂, and then following air exposure. Figure 8(a) shows the variation of sheet resistance in MoS₂ monolayers with a 30 min BuLi immersion time with and without Et₂N surface functionalization. After 30 min BuLi treatment, the n-type doped 2H MoS₂ monolayers have a lower sheet resistance compared to the as-grown 2H MoS₂ for both unfunctionalized and functionalized monolayers [68, 69]. When the BuLi only MoS₂ monolayers are exposed to air for 10 mins, the sheet resistance increases closer to the initial 2H state;

however, the n-type 2H Et₂N-MoS₂ monolayers only have a small change when exposed to air for 10 mins. This result agrees with our previous findings that the Et₂N surface functionalization stabilizes the n-type doping of MoS₂ in air.

We also evaluate the MoS₂ monolayers after being immersed in BuLi for 24 h with and without Et₂N functionalization (figure 8(b)). In these set of measurements, we find very similar trends; however, there is a lower sheet resistance for the 24 h BuLi treatments compared to the 30 min BuLi treatments for both the unfunctionalized and functionalized monolayers in N₂. The lower sheet resistance in N₂ is due to the longer BuLi immersion time that completely converts 2H MoS₂ to 1T' MoS₂. After exposing both monolayers to air for 24 h, the sheet resistance of the BuLi only MoS₂ monolayer increases closer to the initial 2H MoS₂ sheet resistance; in contrast, the 1T' Et₂N-MoS₂ monolayer has only a small increase in sheet resistance. This air exposure highlights how the Et₂N functionalization stabilizes the 1T' MoS₂ monolayers for 24 h in air. Overall, the MoS₂ monolayer R values are ~10⁷ Ω/square and agree with previous MoS₂ monolayer measurements, which range from 10⁷ to 10¹¹ Ω/square [70, 71]. In general, these R values are higher than what is reported for MoS₂ nanosheets [72–74].

In summary, electrical conductance measurements along with our confocal Raman results demonstrate that the immersion time of 2H MoS₂ monolayers in BuLi heavily n-type dope MoS₂ at shorter times and phase convert the MoS₂ to 1T' at longer times. Moreover, the Et₂N surface functionalization stabilizes these heavily n-type doped 2H or 1T' MoS₂ monolayers in air for at least two weeks and likely longer, which will benefit the application of MoS₂ monolayers in advanced electronic devices and energy harvesting.

4. Conclusions

We report on the stabilization of heavily n-type doped 2H and 1T' MoS₂ monolayers with surface functionalization. We find that the BuLi immersion time controls the amount of electron transfer to MoS₂ monolayers on ITO or sapphire substrates, which changes the MoS₂ monolayer electronic structure. Specifically, a 10 min to 120 min BuLi immersion time will heavily n-type dope the 2H MoS₂, whereas phase conversion to 1T' occurs between 2- and 6 h BuLi immersion times. These heavily n-type doped 2H and 1T' MoS₂ monolayers are not stable when exposed to air but slightly oxidize and revert back to the initial 2H state. However, by adding Et₂N surface functional groups to the MoS₂ surface, we stabilize the modified MoS₂ in air. Our microscopic characterization results show that the entire MoS₂ monolayer is homogeneously n-type doped or 1T' phase converted and

stabilized. Chemical control of the electronic structure of MoS₂ monolayers will be important as these monolayers are used in various applications, such as catalysis, batteries, resistors, and sensors. We speculate that this methodology for chemical control can be extended to other 2D transition metal dichalcogenides, opening a broad array of surface functionalization and strategies for the use of 2D materials in novel devices and applications.

Data availability statement

The data that support the findings of this study are available upon reasonable request from the authors.

Acknowledgments

H Z, S U N, N A, Z L, and E M M acknowledge funding provided by U.S. Department of Energy, Office of Science, Office of Basic Energy Sciences, Division of Chemical Sciences, Geosciences and Biosciences, Solar Photochemistry for the overall project direction, material growth and treatments, and all other measurements. The support of the SECM work by the National Science Foundation (CHE-1900463; M V M) is gratefully acknowledged. J H acknowledges support for the 4-point measurements from the Center for Hybrid Organic Inorganic Semiconductors for Energy (CHOISE) an Energy Frontier Research Center funded by the Office of Basic Energy Sciences, Office of Science. T K's internship is supported by the U.S. Department of Energy, Office of Science, Office of Workforce Development for Teachers and Scientists (WDTS) under the Science Undergraduate Laboratory Internship (SULI) program at NREL. The NREL authors would like to thank the Alliance for Sustainable Energy, LLC, the manager and operator of the National Renewable Energy Laboratory for the U.S. Department of Energy under Contract No. DE-AC36-08GO28308. The views expressed in the article do not necessarily represent the views of the Department of Energy or the U.S. Government. The U.S. Government retains and the publisher, by accepting the article for publication, acknowledges that the U.S. Government retains a nonexclusive, paid-up, irrevocable, worldwide license to publish or reproduce the published form of this work, or allow others to do so, for U.S. Government purposes.

ORCID iDs

Sanjini U Nanayakkara  <https://orcid.org/0000-0003-1526-2081>

Nuwan H Attanayake  <https://orcid.org/0000-0001-7622-2337>

Elisa M Miller  <https://orcid.org/0000-0002-7648-5433>

References

- [1] Yadav V, Roy S, Singh P, Khan Z and Jaiswal A 2019 2D MoS₂-based nanomaterials for therapeutic, bioimaging, and biosensing applications *Small* **15** 1803706
- [2] Venkata Subbaiah Y P, Saji K J and Tiwari A 2016 Atomically thin MoS₂: a versatile nongraphene 2D material *Adv. Funct. Mater.* **26** 2046–69
- [3] Sulas-Kern D B, Miller E M and Blackburn J L 2020 Photoinduced charge transfer in transition metal dichalcogenide heterojunctions—towards next generation energy technologies *Energy Environ. Sci.* **13** 2684–740
- [4] Jiang L, Lin B, Li X, Song X, Xia H, Li L and Zeng H 2016 Monolayer MoS₂-graphene hybrid aerogels with controllable porosity for lithium-ion batteries with high reversible capacity *ACS Appl. Mater. Interfaces* **8** 2680–7
- [5] Zhang J, Wu J, Guo H, Chen W, Yuan J, Martinez U, Gupta G, Mohite A, Ajayan P M and Lou J 2017 Unveiling active sites for the hydrogen evolution reaction on monolayer MoS₂ *Adv. Mater.* **29** 1701955
- [6] Luo Y K, Xu J, Zhu T, Wu G, McCormick E J, Zhan W, Neupane M R and Kawakami R K 2017 Opto-valleytronic spin injection in monolayer MoS₂/few-layer graphene hybrid spin valves *Nano Lett.* **17** 3877–83
- [7] Perkins F K, Friedman A L, Cobas E, Campbell P M, Jernigan G G and Jonker B T 2013 Chemical vapor sensing with monolayer MoS₂ *Nano Lett.* **13** 668–73
- [8] Mak K F, Lee C, Hone J, Shan J and Heinz T F 2010 Atomically thin MoS₂: a new direct-gap semiconductor *Phys. Rev. Lett.* **105** 136805
- [9] Chhowalla M, Shin H S, Eda G, Li L-J, Loh K P and Zhang H 2013 The chemistry of two-dimensional layered transition metal dichalcogenide nanosheets *Nat. Chem.* **5** 263–75
- [10] Sercombe D, Schwarz S, Pozo-Zamudio O D, Liu F, Robinson B J, Chekhovich E A, Tartakovskii I I, Kolosov O and Tartakovskii A I 2013 Optical investigation of the natural electron doping in thin MoS₂ films deposited on dielectric substrates *Sci. Rep.* **3** 3489
- [11] Komsa H-P and Krasheninnikov A V 2015 Native defects in bulk and monolayer MoS₂ from first principles *Phys. Rev. B* **91** 125304
- [12] Chae W H, Cain J D, Hanson E D, Murthy A A and David V P 2017 Substrate-induced strain and charge doping in CVD-grown monolayer MoS₂ *Appl. Phys. Lett.* **111** 143106
- [13] Li M, Yao J, Wu X, Zhang S, Xing B, Niu X, Yan X, Yu Y, Liu Y and Wang Y 2020 P-type doping in large-area monolayer MoS₂ by chemical vapor deposition *ACS Appl. Mater. Interfaces* **12** 6276–82
- [14] Xu W, Li S, Zhou S, Lee J K, Wang S, Sarwat S G, Wang X, Bhaskaran H, Pasta M and Warner J H 2018 Large dendritic monolayer MoS₂ grown by atmospheric pressure chemical vapor deposition for electrocatalysis *ACS Appl. Mater. Interfaces* **10** 4630–9
- [15] Zhu J et al 2017 Argon plasma induced phase transition in monolayer MoS₂ *J. Am. Chem. Soc.* **139** 10216–9
- [16] Ye G, Gong Y, Lin J, Li B, He Y, Pantelides S T, Zhou W, Vajtai R and Ajayan P M 2016 Defects engineered monolayer MoS₂ for improved hydrogen evolution reaction *Nano Lett.* **16** 1097–103
- [17] Lin C-P, Chen P-C, Huang J-H, Lin C-T, Wang D, Lin W-T, Cheng C-C, Su C-J, Lan Y-W and Hou T-H 2019 Local modulation of electrical transport in 2D layered materials induced by electron beam irradiation *ACS Appl. Electron. Mater.* **1** 684–91
- [18] Lloyd D, Liu X, Christopher J W, Cantley L, Wadehra A, Kim B L, Goldberg B B, Swan A K and Bunch J S 2016 Band gap engineering with ultralarge biaxial strains in suspended monolayer MoS₂ *Nano Lett.* **16** 5836–41
- [19] Conley H J, Wang B, Ziegler J I, Haglund R F, Pantelides S T and Bolotin K I 2013 Bandgap engineering of strained monolayer and bilayer MoS₂ *Nano Lett.* **13** 3626–30

- [20] Wang Z, Liu X, Zhu J, You S, Bian K, Zhang G, Feng J and Jiang Y 2019 Local engineering of topological phase in monolayer MoS₂ *Sci. Bull.* **64** 1750–6
- [21] Peng J, Liu Y, Luo X, Wu J, Lin Y, Guo Y, Zhao J, Wu X, Wu C and Xie Y 2019 High phase purity of large-sized 1T'-MoS₂ monolayers with 2D superconductivity *Adv. Mater.* **31** 1900568
- [22] Qian X, Liu J, Fu L and Li J 2014 Quantum spin Hall effect in two-dimensional transition metal dichalcogenides *Science* **346** 1344–7
- [23] Zhuang H L, Johannes M D, Singh A K and Hennig R G 2017 Doping-controlled phase transitions in single-layer MoS₂ *Phys. Rev. B* **96** 165305
- [24] Hu T, Li R and Dong J 2013 A new (2 × 1) dimerized structure of monolayer 1T-molybdenum disulfide, studied from first principles calculations *J. Chem. Phys.* **139** 174702
- [25] Li Z, Song Y and Tang S 2020 Quantum spin Hall state in monolayer 1T'-TMDs *J. Phys.: Condens. Matter* **32** 333001
- [26] Yin X et al 2017 Tunable inverted gap in monolayer quasi-metallic MoS₂ induced by strong charge-lattice coupling *Nat. Commun.* **8** 486
- [27] Tian Y, Song X, Liu J, Zhao L, Zhang P and Gao L 2019 Generation of monolayer MoS₂ with 1T phase by spatial-confinement-induced ultrathin PPy anchoring for high-performance supercapacitor *Adv. Mater. Interfaces* **6** 1900162
- [28] Wang Y, Slassi A, Stoeckel M-A, Bertolazzi S, Cornil J, Beljonne D and Samorì P 2019 Doping of monolayer transition-metal dichalcogenides via physisorption of aromatic solvent molecules *J. Phys. Chem. Lett.* **10** 540–7
- [29] Lockhart de La Rosa C J, Phillipson R, Teyssandier J, Adisojoso J, Balaji Y, Huyghebaert C, Radu I, Heyns M, De Feyter S and De Gendt S 2016 Molecular doping of MoS₂ transistors by self-assembled oleylamine networks *Appl. Phys. Lett.* **109** 253112
- [30] Zou H, Zeng Q, Peng M, Zhou W, Dai X and Ouyang F 2018 Electronic structures and optical properties of P and Cl atoms adsorbed/substitutionally doped monolayer MoS₂ *Solid State Commun.* **280** 6–12
- [31] Fang H, Tosun M, Seol G, Chang T C, Takei K, Guo J and Javey A 2013 Degenerate n-doping of few-layer transition metal dichalcogenides by potassium *Nano Lett.* **13** 1991–5
- [32] Dhakal K P, Ghimire G, Chung K, Duong D L, Kim S W and Kim J 2019 Probing multiphased transition in bulk MoS₂ by direct electron injection *ACS Nano* **13** 14437–46
- [33] Li M et al 2020 Air stable and reversible n-type surface functionalization of MoS₂ monolayer using Arg and Lys amino acids *J. Mater. Chem. C* **8** 12181–8
- [34] Ogura H et al 2021 Air-stable and efficient electron doping of monolayer MoS₂ by salt–crown ether treatment *Nanoscale* **13** 8784–9
- [35] Lukowski M A, Daniel A S, Meng F, Forticaux A, Li L and Jin S 2013 Enhanced hydrogen evolution catalysis from chemically exfoliated metallic MoS₂ nanosheets *J. Am. Chem. Soc.* **135** 10274–7
- [36] Sun D et al 2019 1T MoS₂ nanosheets with extraordinary sodium storage properties via thermal-driven ion intercalation assisted exfoliation of bulky MoS₂ *Nano Energy* **61** 361–9
- [37] Knirsch K C et al 2015 Basal-plane functionalization of chemically exfoliated molybdenum disulfide by diazonium salts *ACS Nano* **9** 6018–30
- [38] Benson E E, Zhang H, Schuman S A, Nanayakkara S U, Bronstein N D, Ferrere S, Blackburn J L and Miller E M 2018 Balancing the hydrogen evolution reaction, surface energetics, and stability of metallic MoS₂ nanosheets via covalent functionalization *J. Am. Chem. Soc.* **140** 441–50
- [39] Radisavljevic B, Radenovic A, Brivio J, Giacometti V and Kis A 2011 Single-layer MoS₂ transistors *Nat. Nano* **6** 147–50
- [40] Voiry D, Goswami A, Kappera R, Silva C D C E, Kaplan D, Fujita T, Chen M, Asefa T and Chhowalla M 2015 Covalent functionalization of monolayered transition metal dichalcogenides by phase engineering *Nat. Chem.* **7** 45–49
- [41] Dines M B 1975 Lithium intercalation via n-Butyllithium of the layered transition metal dichalcogenides *Mater. Res. Bull.* **10** 287–91
- [42] Yun S J, Han G H, Kim H, Duong D L, Shin B G, Zhao J, Vu Q A, Lee J, Lee S M and Lee Y H 2017 Telluriding monolayer MoS₂ and WS₂ via alkali metal scooter *Nat. Commun.* **8** 2163
- [43] Yu H et al 2017 Wafer-scale growth and transfer of highly-oriented monolayer MoS₂ continuous films *ACS Nano* **11** 12001–7
- [44] Sun T, Zhang H, Wang X, Liu J, Xiao C, Nanayakkara S U, Blackburn J L, Mirkin M V and Miller E M 2019 Nanoscale mapping of hydrogen evolution on metallic and semiconducting MoS₂ nanosheets *Nanoscale Horiz.* **4** 619–24
- [45] Zhang X, Qiao X-F, Shi W, Wu J-B, Jiang D-S and Tan P-H 2015 Phonon and Raman scattering of two-dimensional transition metal dichalcogenides from monolayer, multilayer to bulk material *Chem. Soc. Rev.* **44** 2757–85
- [46] Li H, Zhang Q, Yap C C R, Tay B K, Edwin T H T, Olivier A and Baillargeat D 2012 From bulk to monolayer MoS₂: evolution of Raman scattering *Adv. Funct. Mater.* **22** 1385–90
- [47] Attanayake N H, Thenuwara A C, Patra A, Aulin Y V, Tran T M, Chakraborty H, Borguet E, Klein M L, Perdew J P and Strongin D R 2018 Effect of intercalated metals on the electrocatalytic activity of 1T-MoS₂ for the hydrogen evolution reaction *ACS Energy Lett.* **3** 7–13
- [48] Yu Y et al 2018 High phase-purity 1T'-MoS₂—and 1T'-MoSe₂-layered crystals *Nat. Chem.* **10** 638–43
- [49] Kiriya D, Tosun M, Zhao P, Kang J S and Javey A 2014 Air-stable surface charge transfer doping of MoS₂ by benzyl viologen *J. Am. Chem. Soc.* **136** 7853–6
- [50] Martinová J, Otyepka M and Lazar P 2020 Oxidation of metallic two-dimensional transition metal dichalcogenides: 1T-MoS₂ and 1T-TaS₂ *2D Mater.* **7** 045005
- [51] Jeon J, Jang S K, Jeon S M, Yoo G, Jang Y H, Park J-H and Lee S 2015 Layer-controlled CVD growth of large-area two-dimensional MoS₂ films *Nanoscale* **7** 1688–95
- [52] Dhakal K P, Duong D L, Lee J, Nam H, Kim M, Kan M, Lee Y H and Kim J 2014 Confocal absorption spectral imaging of MoS₂: optical transitions depending on the atomic thickness of intrinsic and chemically doped MoS₂ *Nanoscale* **6** 13028–35
- [53] Carroll G M, Zhang H, Dunklin J R, Miller E M, Neale N R and van de Lagemaat J 2019 Unique interfacial thermodynamics of few-layer 2D MoS₂ for (photo)electrochemical catalysis *Energy Environ. Sci.* **12** 1648–56
- [54] Jiao Y, Hafez A M, Cao D, Mukhopadhyay A, Ma Y and Zhu H 2018 Metallic MoS₂ for high performance energy storage and energy conversion *Small* **14** 1800640
- [55] Birmingham B, Yuan J, Filez M, Fu D, Hu J, Lou J, Scully M O, Weckhuysen B M and Zhang Z 2019 Probing the effect of chemical dopant phase on photoluminescence of monolayer MoS₂ using *in situ* Raman microspectroscopy *J. Phys. Chem. C* **123** 15738–43
- [56] Li S et al 2019 Enhanced performance of a CVD MoS₂ photodetector by chemical *in situ* n-type doping *ACS Appl. Mater. Interfaces* **11** 11636–44
- [57] Kaushik N, Karmakar D, Nipane A, Karande S and Lodha S 2016 Interfacial n-doping using an ultrathin TiO₂ layer for contact resistance reduction in MoS₂ *ACS Appl. Mater. Interfaces* **8** 256–63
- [58] Chang K, Hai X, Pang H, Zhang H, Shi L, Liu G, Liu H, Zhao G, Li M and Ye J 2016 Targeted synthesis of 2H- and 1T-phase MoS₂ monolayers for catalytic hydrogen evolution *Adv. Mater.* **28** 10033–41
- [59] Liang Y and Yang L 2015 Carrier plasmon induced nonlinear band gap renormalization in two-dimensional semiconductors *Phys. Rev. Lett.* **114** 063001
- [60] Yao K, Yan A, Kahn S, Suslu A, Liang Y, Barnard E S, Tongay S, Zettl A, Borys N J and Schuck P J 2017 Optically discriminating carrier-induced quasiparticle band gap and

- exciton energy renormalization in monolayer MoS₂ *Phys. Rev. Lett.* **119** 087401
- [61] Rao R, Islam A E, Singh S, Berry R, Kawakami R K, Maruyama B and Katoch J 2019 Spectroscopic evaluation of charge-transfer doping and strain in graphene/MoS₂ heterostructures *Phys. Rev. B* **99** 195401
- [62] Yau S, Lee Y, Chang C, Fan L, Yang Y and Dow W-P 2009 Structures of aniline and polyaniline molecules adsorbed on Au(111) electrode: as probed by *in situ* STM, *ex situ* XPS, and NEXAFS *J. Phys. Chem. C* **113** 13758–64
- [63] Nanayakkara S U, van de Lagemaat J and Luther J M 2015 Scanning probe characterization of heterostructured colloidal nanomaterials *Chem. Rev.* **115** 8157–81
- [64] Guo C *et al* 2017 Observation of superconductivity in 1T'-MoS₂ nanosheets *J. Mater. Chem. C* **5** 10855–60
- [65] Saigal N, Wielert I, Čapeta D, Vujičić N, Senkovskiy B V, Hell M, Kralj M and Grüneis A 2018 Effect of lithium doping on the optical properties of monolayer MoS₂ *Appl. Phys. Lett.* **112** 121902
- [66] Leng K, Chen Z, Zhao X, Tang W, Tian B, Nai C T, Zhou W and Loh K P 2016 Phase restructuring in transition metal dichalcogenides for highly stable energy storage *ACS Nano* **10** 9208–15
- [67] Wu M, Zhan J, Wu K, Li Z, Wang L, Geng B, Wang L and Pan D 2017 Metallic 1T MoS₂ nanosheet arrays vertically grown on activated carbon fiber cloth for enhanced Li-ion storage performance *J. Mater. Chem. A* **5** 14061–9
- [68] Jiang L, Zhang S, Kulinich S A, Song X, Zhu J, Wang X and Zeng H 2015 Optimizing hybridization of 1T and 2H phases in MoS₂ monolayers to improve capacitances of supercapacitors *Mater. Res. Lett.* **3** 177–83
- [69] Li S-L, Komatsu K, Nakaharai S, Lin Y-F, Yamamoto M, Duan X and Tsukagoshi K 2014 Thickness scaling effect on interfacial barrier and electrical contact to two-dimensional MoS₂ layers *ACS Nano* **8** 12836–42
- [70] Gao H *et al* 2020 Tuning electrical conductance of MoS₂ monolayers through substitutional doping *Nano Lett.* **20** 4095–101
- [71] Mazzoni A L, Burke R A, Chin M L and Hwee M J 2017 *Effects of Growth Conditions on the Measured Electrical Properties of Monolayer Molybdenum Disulfide* p 50
- [72] Hamada T, Tomiya S, Tatsumi T, Hamada M, Horiguchi T, Kakushima K, Tsutsui K and Wakabayashi H 2021 Sheet resistance reduction of MoS₂ film using sputtering and chlorine plasma treatment followed by sulfur vapor annealing *IEEE J. Electron Devices Soc.* **9** 278–85
- [73] Wan J, Lacey S D, Dai J, Bao W, Fuhrer M S and Hu L 2016 Tuning two-dimensional nanomaterials by intercalation: materials, properties and applications *Chem. Soc. Rev.* **45** 6742–65
- [74] Lan L, Chen D, Yao Y, Peng X, Wu J, Li Y, Ping J and Ying Y 2018 Phase-dependent fluorescence quenching efficiency of MoS₂ nanosheets and their applications in multiplex target biosensing *ACS Appl. Mater. Interfaces* **10** 42009–17